Supporting Information

Bounoutas et al. 10.1073/pnas.1101360108

SI Materials and Methods

Quantification of Fluorescence. For animals expressing fluorescent transgenes, ALM neurons from young, gravid adults grown at 20 °C were photographed at 63× magnification and the same exposure. We measured the maximum intensity of GFP-expressing cell bodies using ImageJ 1.40g (http://rsb.info.nih.gov/ij/). For quantifying intensity of MEC-2 immunostaining of cell bodies, we photographed ALM neurons from young, gravid adults grown at 20 °C at 40× magnification and the same exposure. JPEG images were cropped identically and rotated to position the cell bodies in the same orientation. Because intensity of MEC-2 and background fluorescence varies with immunostaining, we used ImageJ to measure the integrated density of intensity of a 100 × 25 pixel rectangle containing the cell body; to normalize each sample for background, we subtracted the minimum intensity value multiplied by the same pixel area. The remaining integrated density was divided by 100,000 to generate the value for each animal.

Quantitative PCR. We isolated total RNA from animals using TRI reagent (Molecular Research Center) according to the manufacturer's instructions. mRNA was purified from 50 μg of total RNA with Oligotex mRNA mini kit (Qiagen) and reverse-transcribed into cDNA using Quantitect Reverse Transcription kit (Qiagen). Each real-time PCR was performed with 50 ng of sample cDNA in a 25-μL reaction using Quantifast SYBR Green PCR kit (Qiagen) and a 7300 real-time PCR system (Applied Biosystems). Standard curves for each transcript was determined using serially diluted samples of genomic DNA. The ratio of message levels comparing experimental samples to wild type for each gene were calculated as described (1) and normalized to the levels of *ama-1* transcripts. Primers for *mec-18* and *mec17* transcripts included a small intron sequence, and the size of the PCR products from cDNA were verified by gel electrophoresis to ensure that no genomic DNA was present.

Genetic Mapping of Mutants. Three factor crosses of *u818; uIs43* with *dpy-5(e61)* and *unc-75(e950)* as well as deletion mapping with *dxDf2* and *eDf3* narrowed the position of the *u818* mutation to the right arm of chromosome I. Snip-SNP mapping (2) of recombinants between the Hawaiian strain CB4856 and *dpy-24 u818; uIs43* and *u818 unc-59; uIs43* double mutants further narrowed the position of *u818* locus to a 380-kb region covered by 16 cosmids between map positions 13.19 and 14.00. We sequenced candidate genes in the region, and all six noncomplementing mutations produced mutations in the reading frame of *dlk-1*: *u815* G2778A G308E; *u816* G2189A G144R; *u817* C2300T Q181Stop; *u818* C2244T Q166Stop; *u820* G2495A D246N; *u821* Δ3505–3569, G3616A frameshift (resulting in a premature stop at codon 455). Noncomplementation with the preexisting *dlk-1(km12)* allele and TRN-specific rescue of the *u818* mutation confirmed the identify of the gene. TRN-specific rescue of *dlk-1(u818); uIs44* was performed via injection (1 ng/μL) of a plasmid expressing $P_{mec\text{-}18}$*dlk-1*; 500 bases of the *mec-18* promoter upstream from the start of translation were inserted into the HindIII BamHI sites in pBSKII(+), and the wild-type *dlk-1* coding sequence (with 1.25 kb of downstream DNA) was inserted immediately thereafter into SpeI EagI sites.

Similarly, the position of *u819* was mapped to the X chromosome and further narrowed by noncomplementation with the deletion *meDf6*. Following a suggestion from Yishi Jin, we tested whether *cebp-1*, a gene in the region, was defective, and the *u819* mutation encoded an A285V change. Noncomplementation of *u819* with *cebp-1(tm2807)* and rescue by TRN-specific *cebp-1(+)* confirmed the identity of the gene. TRN-specific rescue of *uIs44; cebp-1(u818)* was performed via injection (1 ng/μL) of a plasmid expressing $P_{mec\text{-}18}$*cebp-1*; 500 bases of the *mec-18* promoter upstream from the start of translation were inserted into the HindIII BamHI sites in pBSKII(+), and the wild-type *cebp-1* coding sequence (with 810 bases of downstream DNA) was inserted immediately thereafter into XbaI EagI sites.

1. Morrison TB, Weis JJ, Wittwer CT (1998) Quantification of low-copy transcripts by continuous SYBR Green I monitoring during amplification. *Biotechniques* 24:954–958, 960, 962.

2. Wicks SR, Yeh RT, Gish WR, Waterston RH, Plasterk RH (2001) Rapid gene mapping in *Caenorhabditis elegans* using a high density polymorphism map. *Nat Genet* 28: 160–164.

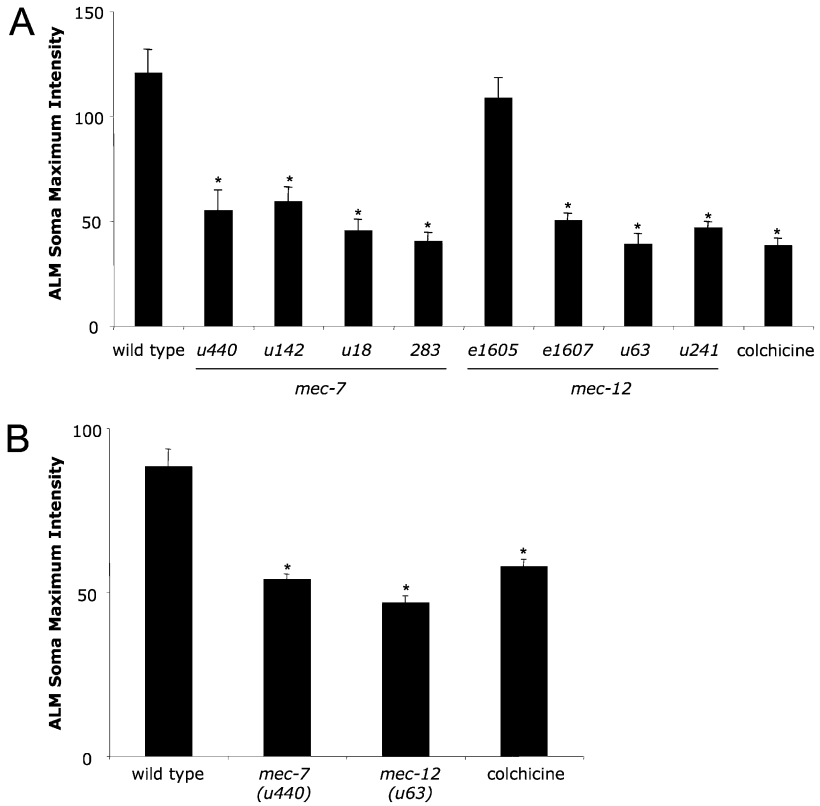

Fig. S1. Quantification of fluorescence reduction in GFP-expressing TRNs in *mec-7* and *mec-12* mutants. Maximum intensity of GFP fluorescence in ALM cell bodies of animals expressing (*A*) *uIs22* ($P_{mec\text{-}3}gfp$) and (*B*) *uIs57* ($P_{unc\text{-}119}gfp$) transgenes. The mean ± SEM is indicated; n = 10 cells for *A* and 8 cells for *B*. *$P \leq 0.05$ difference from wild type, here and in subsequent figures.

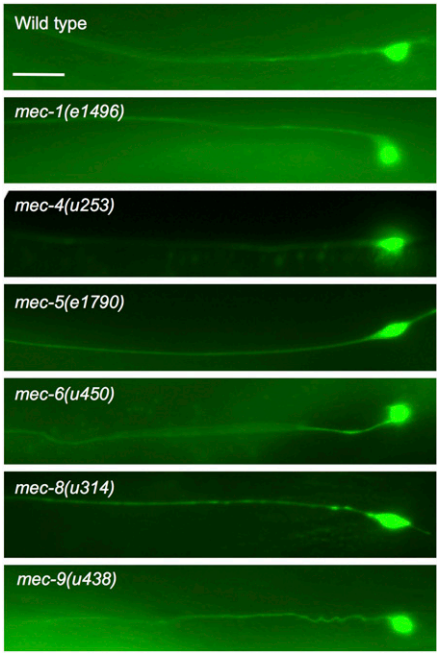

Fig. S2. Mutations in other TRN-specific genes do not reduce GFP fluorescence. ALM neurons in adult wild type, *mec-1, mec-4, mec-5, mec-6, mec-8,* and *mec-9* animals expressing *uIs22* ($P_{mec\text{-}3}gfp$). (Scale bar, 20 μm.)

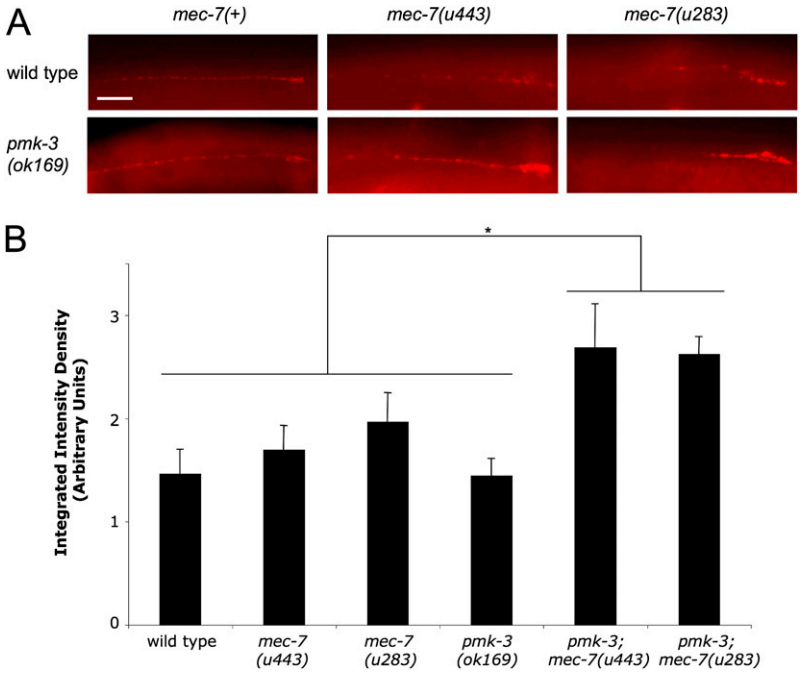

Fig. S3. Cre mutations increase MEC-2 levels in TRN cell bodies of tubulin mutants but do not rescue transport defects. (*A*) Representative pictures of immunostaining against MEC-2 in ALM neurons of young adult wild-type animals, *mec-7* recessive (*u443*) and dominant (*u283*) mutants, *pmk-3(ok169)* mutants, and *pmk-3; mec-7* double mutants. (*B*) Integrated density of intensity of MEC-2 immunostaining in TRN cell bodies. The mean ± SEM is indicated; $n = 12$ cell bodies for each genotype. Values for *mec-7(u443)*, *mec-7(u283*), and *pmk-3(ok169)* are not statistically different from wild type or each other. (Scale bar, 20 μm.)

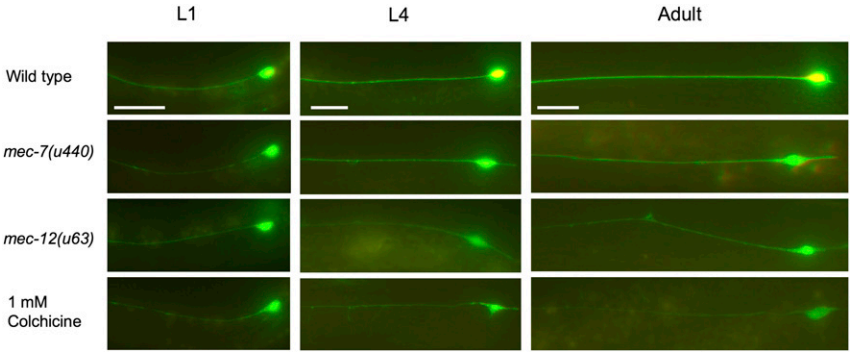

Fig. S4. Tubulin mutations and colchicine reduce MEC-17::GFP fluorescence in a time-dependent manner. Fluorescence from MEC-17::GFP in ALM neurons of wild type, *mec-7(u440)*, *mec-12(u63)*, and colchicine treated was measured in L1 larvae, L4 larvae, and adults 48 h after hatching. (Scale bars, 20 μm.)

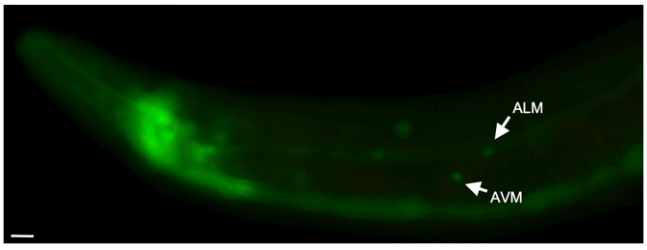

Fig. S5. *mec-3* adults express GFP from the *unc-119* promoter in cells that would normally differentiate as TRNs ("ALM" and "AVM"). (Scale bar, 20 μm.)

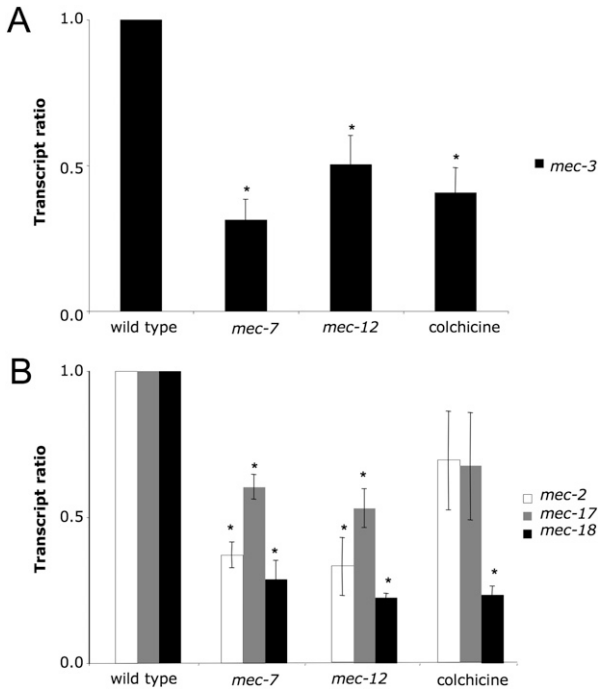

Fig. S6. Microtubule defects reduce steady-state mRNA levels of TRN-specific genes. (*A*) Transcripts for *mec-3* (normalized to the level of *ama-1*) were measured in L4 larvae from wild type, *mec-7(u443)*, and *mec-12(u63)* mutants, and colchicine-treated wild-type animals. Results are compared setting the wild-type levels to 1.0. The mean ± SEM is indicated; $n \geq 3$ independent experiments for each transcript. (*B*) Transcript ratios for *mec-2*, *mec-17*, and *mec-18* determined and presented as in *A*.

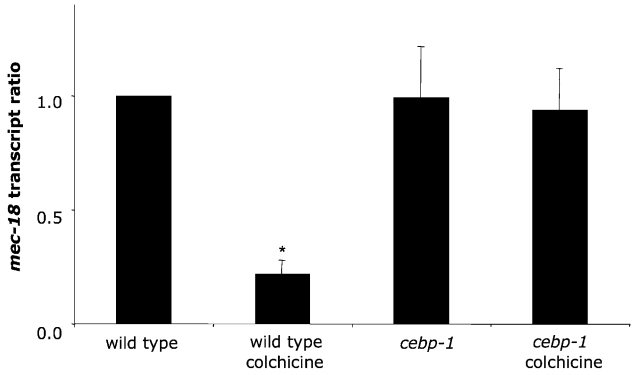

Fig. S7. Reduction of steady-state mRNA levels is CEBP-1 dependent. Transcripts for *mec-18* (normalized to the level of *ama-1*) were measured in L4 larvae from wild-type and *cebp-1(tm2807)* animals grown on control and 1-mM colchicine plates. Results are compared setting the wild-type control levels to 1.0. The mean ± SEM is indicated; $n \geq 5$ independent experiments for each transcript.

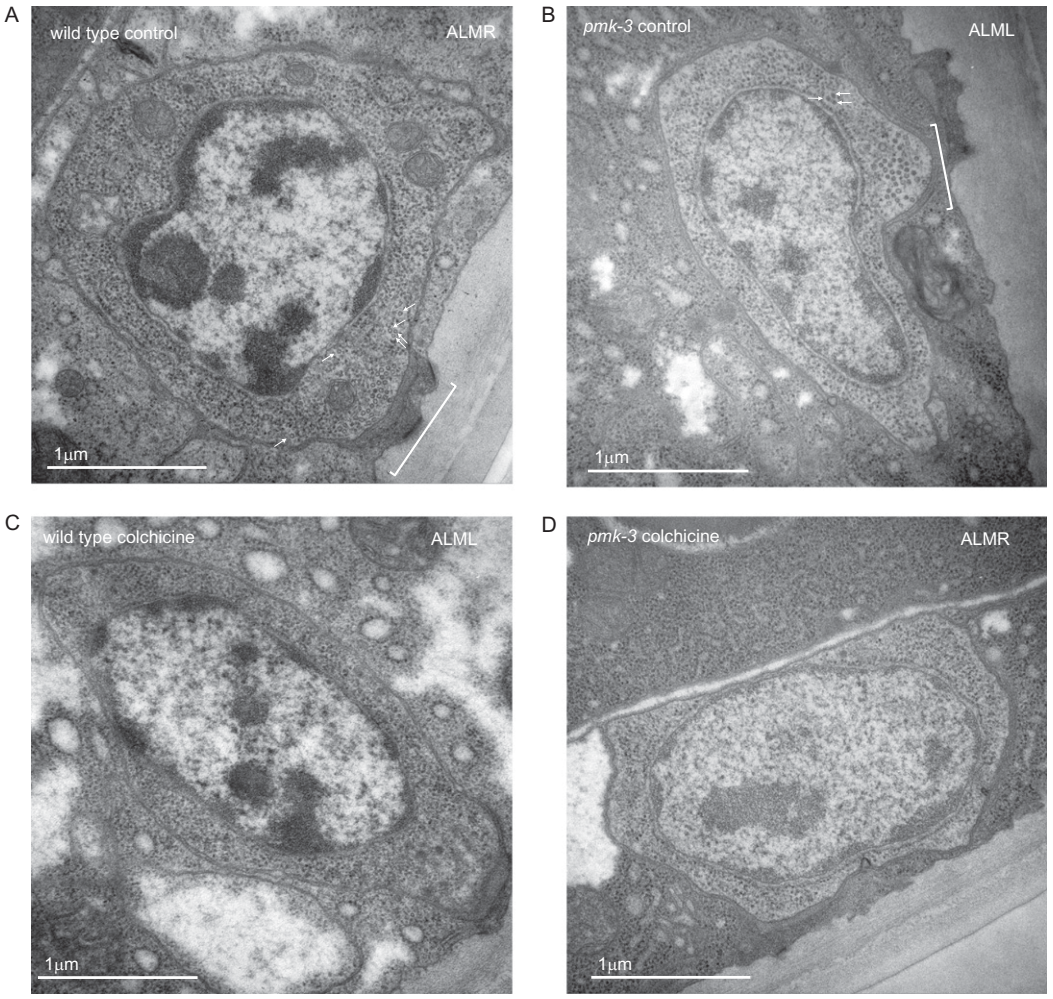

Fig. S8. Colchicine treatment depolymerizes TRN microtubules in wild-type and *pmk-3* mutants. Electron micrographs of ALM neurons from control (*A*) wild type and (*B*) *pmk-3(ok169)* and colchicine-treated (*C*) wild-type and (*D*) *pmk-3* animals. White brackets indicate the TRN microtubule bundle near the extracellular mantle, and white arrows indicate TRN microtubules located outside of the bundle. Note that depolymerization of the bundle by cochicine does not destabilize the mantle (*Lower Right* corner in *C*; *Lower* border in *D*). (Scale bars, 1 μm.)